



RESEARCH ARTICLE

Magnetic Resonance in Medicine

Adiabatic null passage for on-resonance magnetization transfer preparation

Shahrokh Abbasi-Rad^{1,2,3,4}  | David G. Norris^{1,2} 

¹Donders Institute for Brain, Cognition and Behaviour, Donders Centre for Cognitive Neuroimaging, Radboud University Nijmegen, Nijmegen, Netherlands

²Erwin L. Hahn Institute for Magnetic Resonance Imaging, University Duisburg-Essen, Essen, Germany

³Department of Radiology, Harvard Medical School, Boston, Massachusetts, USA

⁴Athinoula A. Martinos Center for Biomedical Imaging, Massachusetts General Hospital, Charlestown, Massachusetts USA

Correspondence

Shahrokh Abbasi-Rad, Athinoula A. Martinos Center for Biomedical Imaging, Massachusetts General Hospital, Charlestown, MA 02129, USA.
Email: sabbasi-rad@mgh.harvard.edu

Abstract

Purpose: We propose a novel RF pulse providing an adiabatic null passage (ANP) for magnetization transfer preparation with improved insensitivity to B_1^+ and B_0 inhomogeneities and mitigated direct saturation and T_2 effects.

Method: The phase modulation function of a 6-ms time-resampled frequency offset-corrected pulse was modified to achieve zero flip angle at the end of the pulse. The spectral response was simulated, and its insensitivity to B_0 and B_1^+ was investigated and compared with a phase-inverted ($1\bar{2}1-1\bar{2}1$) binomial pulse. The proposed pulse was implemented in a 2D-EPI pulse sequence to generate magnetization transfer (MT) contrast and MT ratio (MTR) maps. In vivo experiments were performed on 3 healthy participants with power-matched settings for ANP and the binomial pulse with the following parameters: 6-ms binomial pulse with a flip angle of 107° (shortest element) and pulse repetition period (PRP) of $TR_{\text{slice}} = 59$ ms, three experiments with 6-ms ANP and constant MT used overdrive factor (OF)/PRP values of $1/TR_{\text{slice}}$, $\sqrt{2}/2TR_{\text{slice}}$, and $\sqrt{3}/3TR_{\text{slice}}$.

Results: At gray matter (white matter) in vivo, the MTR decreased from 61% (64%) at $OF=1$ to 38% (42%) applying ANP with an $OF = \sqrt{3}$ and $PRP = 3 TR_{\text{slice}}$, demonstrating the mitigation of T_2 /direct effect by 22% (22%). Bloch-McConnell simulations gave similar values. In vivo experiments showed significant improvement in the MTR values for areas with high B_0 inhomogeneity.

Conclusion: ANP pulse was shown to be advantageous over its binomial counterpart in providing MT contrast by mitigating the T_2 effect and direct saturation of the liquid pool as well as reduced sensitivity to B_1^+ and B_0 inhomogeneity.

KEYWORDS

adiabatic null passage, direct saturation, magnetization transfer, T_2 effect

1 | INTRODUCTION

The phenomenon of magnetization transfer (MT) is understood by the mechanism of cross-relaxation of water protons (free proton pool) as a result of the exchangeable spin environment established by the macromolecules (bound proton pool), and was first explored in the late 1970s.¹⁻³ Quantitative attempts then followed through the saturation transfer technique proposed by Forsen and Hoffman⁴ to characterize this phenomenon by measuring the underlying transfer rates and macroscopic relaxation times.⁵⁻⁹ Wolff and Balaban were the first to show its macroscopic bulk effect. They produced *in vivo* magnetization transfer contrast (MTC) images by combining the saturation transfer technique with routine imaging procedures.¹⁰

MTC is generated by selectively saturating the bound pool existing in the structure of macromolecules, ideally without directly affecting the mobile long- T_1/T_2 free pool. As a result of this selective saturation, the magnetization exchange between the two pools results in a reduction in the free pool magnetization (M_{sat}), which would relax with a new relaxation rate ($R_{1,\text{sat}}$) if it were excited.¹⁰ Depending on the pulse sequence and the readout, one can generate two different variants (proton density or T_1 weighted) of the MTC.¹¹⁻¹³

The reduced signal of the magnetization transfer (MT)-sensitive tissues (with a higher concentration of macromolecules such as muscle, brain, and cartilage) in contrast to the (almost) intact signal of the MT-insensitive tissues (with no or little concentration of macromolecules such as blood, cerebrospinal, or synovial fluid) leads to interesting clinical applications. Several examples are blood versus background tissue in intracranial MR angiography,¹⁴ cartilage versus joint fluid in intra-articular cartilage evaluation,¹⁵ and spinal cord versus CSF for diagnosing degenerative disc disease in spine imaging.¹⁶

However, MT preparation is not straightforward to implement. Early MTC images were obtained using low-intensity (4–10 μT) continuous-wave RF irradiation with a carrier frequency of up to 20 kHz far from the Larmor frequency of hydrogen.^{10,17} This required the use of auxiliary (decoupler) RF amplifiers and a second RF frequency channel, and had practical limitations regarding high-power deposition.^{15,18} Dixon et al. showed that the MT effect could be detected, incidentally, in routine 2D multislice imaging as a result of the off-resonance RF pulses used for slice selection.¹⁹ The observed incidental MT as a result of pulsed RF provided perspective on the introduction of pulsed MT as an alternative to the continuous-wave RF, which required hardware modifications.

Pulsed MT falls under two categories: (i) off-resonance MT using shaped, narrow-bandwidth, long pulse, which

exploits the difference in the spectral width of the pools,²⁰⁻²⁴ and (ii) on-resonance MT using short pulse with binomial modulation,²⁵ which directly relies on the transfer of magnetization between the pools.^{26,27} Comparison studies between the two classes were performed^{28,29} to compare the efficiency of the resultant MTC images. Thorough optimization studies were done on selecting binomial pulse parameters such as duration, peak amplitude, number of subpulses, duty cycle, phase modulation scheme, and flip angle to achieve the best pool selectivity and minimum energy deposition.³⁰⁻³³ The conclusion was that the binomial pulses, with optimum parameters, produce MTC in a more energy-efficient manner. However, there are two different mechanisms that compromise the efficiency of on-resonance magnetization preparation using binomial pulses: (i) direct saturation of the free pool and (ii) T_2 relaxation during preparation.²⁸ Both lead to the reduction of the available magnetization, which could therefore be mistakenly interpreted as the MT-induced effect.

Binomial-pulse modulation uses the jump-and-return strategy (1- $\bar{1}$), in which the spins are excited by a certain flip angle in one direction and immediately with the same flip angle in the opposite direction, leaving the free pools untouched due to the net zero flip angle while saturating the bound pool protons. However, the second subpulse does not always flip the free pool protons back to equilibrium, leaving a certain amount of magnetization on the transverse plane. This unwanted direct saturation happens due to two main reasons: (i) RF pulse instabilities including an imbalance in binomial pulse timing, distortion in the RF amplifier, incidental inconsistencies in phase or amplitude modulation in the transmitter system, and RF pulse drooping; and (ii) establishment of the effective field for the off-resonance spins, which makes binomial pulses vulnerable to B_0 inhomogeneities.²⁷

Another effect is the reduction in magnetization due to T_2 relaxation. To establish the saturation state for the bound pool while imaging, the MT preparation module is interleaved with the imaging sequence and is applied repeatedly, leaving a small amount of magnetization reduction through T_2 relaxation at each application of the pulse. The accumulated reduction at the end of the imaging sequence could be significant and misinterpreted as MT-induced reduction.

In this study, we use the B_0 insensitivity of the frequency offset-corrected family of adiabatic pulses and their insensitivity to B_1^+ amplitude to explore their selective saturation performance compared with that of the binomial pulses. Hence, we propose a new class of adiabatic pulses generating a zero flip angle, referred to as an adiabatic null passage pulse. We exploit the adiabaticity of these pulses so that we can apply them less often

compared with their binomial counterpart, to achieve the same MT performance but with a reduced T_2 effect. We expect that the adiabatic null passage pulses improve MTC performance by (i) reducing the excessive direct saturation compared with the conventional binomial pulse in areas with high B_0 inhomogeneity, (ii) reducing the sensitivity to variations in B_1^+ amplitude, (iii) allowing the manipulation of the MT effect without necessarily having to modify the pulse duration, and (iv) minimizing the T_2 effect by allowing the use of short high-power pulses applied less frequently.

2 | THEORY

To understand the dynamics of the spins as being manipulated by an adiabatic pulse, we consider an uncoupled spin- $1/2$ system exposed to an external static magnetic field ($\vec{B} = B_0 \vec{k}'$) in a rotating frame of reference with the unit vectors $\vec{i}', \vec{j}', \vec{k}'$. In the presence of an RF pulse applied in the transverse plane with the carrier frequency of ω_{rf} , the bulk magnetization vector precesses about an effective magnetic field formulated as the following equation³⁴ and shown in Figure 1A:

$$\vec{B}_{\text{eff}} = \frac{\Delta\omega}{\gamma} \vec{k}' + B_1(t) \vec{i}' \quad (1)$$

where $B_1(t)$ is the amplitude of the RF pulse; γ is the gyromagnetic ratio; and $\frac{\Delta\omega}{\gamma} \vec{k}'$ is a fictitious field component appearing in the rotating frame,³⁵ indicating the degree of off-resonance.

In the case of conventional amplitude-modulated (AM) pulses, the ω_{rf} is not time-varying; hence, the z-component of the effective field is fixed during the pulse. However, adiabatic RF pulses use both frequency modulation (FM) and AM:

$$B_{\text{rf}}(t) = B_1(t) e^{-i\omega_f(t)t} \quad (2)$$

Therefore, in the adiabatic scenario, both z-components and transverse-plane components of the effective field are time-varying, and they can be fully controlled by the modulation functions (AM/FM). During this movement, the effective field changes its orientation at the rate of $|\frac{d\psi(t)}{dt}|$, where $\psi(t)$ (Figure 1A) is the angle between \vec{k}' and $\vec{\omega}$ vectors, and the bulk magnetization (\vec{M}) precesses around the effective field at the frequency of $\vec{\omega}(t) = \gamma |\vec{B}_{\text{eff}}(t)|$ (Figure 1A). Given that the movement of the effective field is much slower than the precession of the M vector around it, the spin manipulation happens adiabatically, and M follows the trajectory of B_{eff} during the whole passage. This is called the adiabatic condition

and is formulated as follows³⁶:

$$|\frac{d\psi(t)}{dt}| \ll |\omega_{\text{eff}}(t)| \quad (3)$$

Therefore, by designing the AM and FM functions, we can arbitrarily move the ω_{eff} vector, while ensuring that the pulse is working above its adiabatic threshold. An adiabatic full passage (AFP) uses symmetric AM/FM functions that make the effective field start from parallel with B_0 , crossing the origin at the midpoint, and end antiparallel with B_0 .³⁷ In 1998, Norris³⁸ proposed that by simply reversing the phase of the pulse halfway through its time course, the effective field would return to being parallel with B_0 , resulting in a zero tip angle. He proposed this idea to solve the problem of unequal MT between the control and labeling experiments of multislice perfusion imaging.

Here, we extend this theory to tweak the time-resampled frequency offset-corrected (TR-FOCI) RF pulse, which is specific absorption rate (SAR)-efficient as well as robust to B_0/B_1^+ inhomogeneities.³⁹

We added π to the second half of the phase-modulation function of the pulse. In this way, at the midpoint of the time course, the effective field changes its direction and starts taking the reverse orientation, which ends up being parallel to the B_0 . Hence, we termed it an “adiabatic null passage” (ANP). The trajectory of the effective field in an ω_{rf} -rotating frame is depicted for the ANP pulse and is compared with its AFP counterpart in Figure 1B,C, respectively.

Figure 2 shows the spectral response of a 6-ms TR-FOCI pulse for both ANP and AFP scenarios simulated by solving the Bloch equations. We proposed that this pulse is a good candidate for on-resonance MT preparation, and we compared its performance with the currently used pulse, which is phase-inverted $1\bar{2}1\text{-}1\bar{2}1$ binomial pulse preparation.

3 | METHODS

3.1 | RF pulse design

A 6-ms TR-FOCI adiabatic pulse³⁹ was designed for nonselective inversion of the spins. The TR-FOCI pulse uses the hyperbolic secant as the basis function and then exploits reshaping⁴⁰ and resampling⁴¹ functions for optimum spin manipulation with minimum energy deposition. In total, 11 parameters (A_{max} , w , r_1 , r_2 , r_3 , r_4 , r_5 , μ , β , τ_1 , and τ_2) characterize the pulse waveforms uniquely. The values of A_{max} , w , r_1 , r_2 , r_3 , r_4 , and r_5 determine the reshaping function μ and β the hyperbolic secant function, and τ_1 and τ_2 the time-resampling function. These parameters

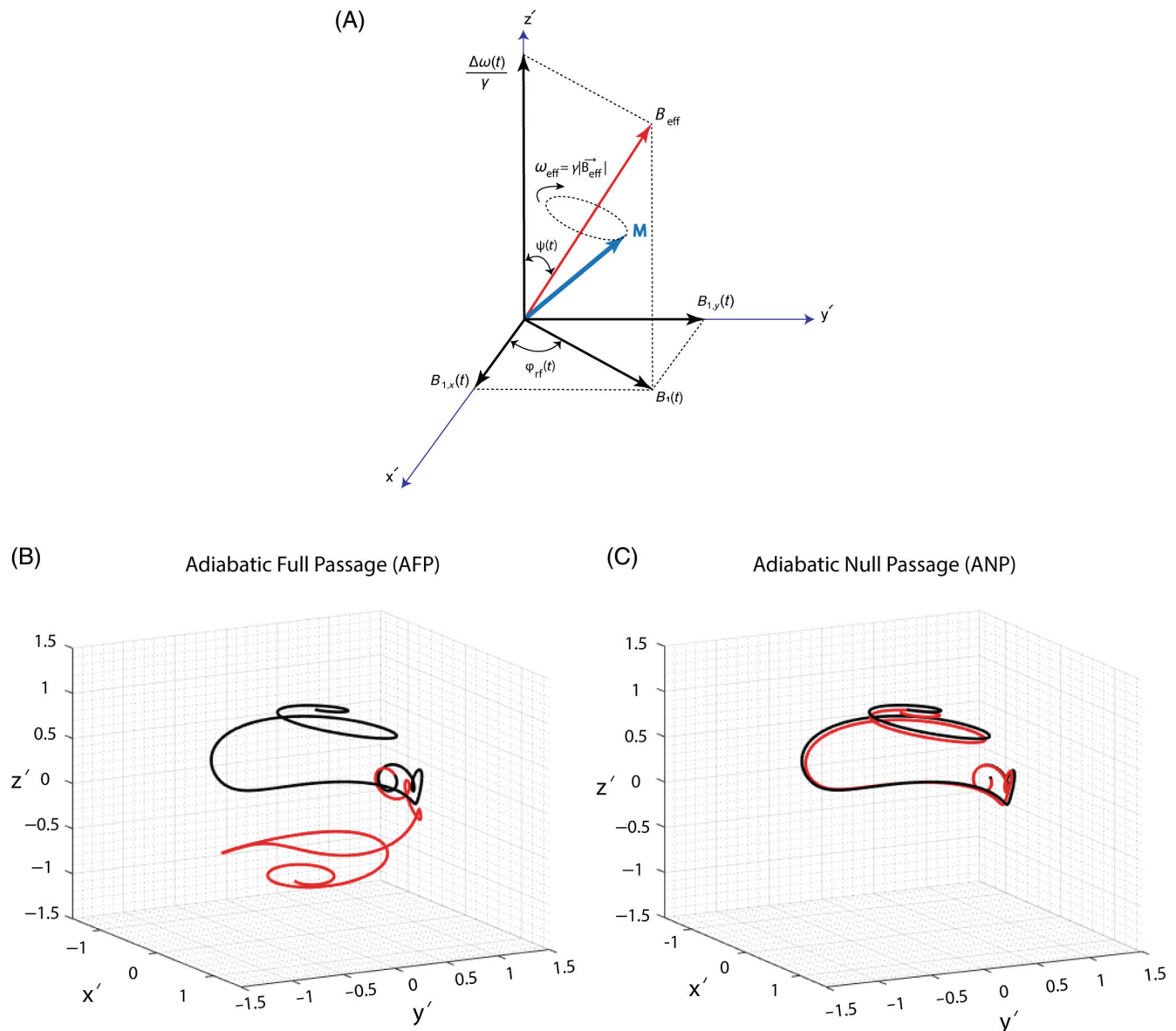


FIGURE 1 (A) Precession of the bulk magnetization vector, M , about the effective-field vector, ω_{eff} , in the ω_{rf} -rotating frame of reference. The key concept of this illustration is to demonstrate the ability to control the locus of the effective-field vector by manipulating its transverse-plane component through the RF pulse amplitude-modulation function and its z -component through the RF pulse frequency/phase-modulation function. The journey of the effective field during the course of a 6-ms time-resampled frequency offset-corrected adiabatic pulse is depicted with full passage (B) and null passage (C). The first half of the trajectory is in black, and the second half is in red. Note that the red part of the trajectory in (B) is reversed in (C) due to adding π to the phase modulation function.

were optimized using genetic and greedy hill-climbing algorithms. The optimization process is described briefly in Abbasi-Rad et al.⁴² The phase modulation function of the designed inversion pulse was then modified by adding a π phase offset to the second half of its time course to achieve the null passage. The optimized values were as follows: 8.01, 0.44, 0.79, 0.45, 0.89, 0.42, 0.97, 1.41, 4.59, 0.31, and 0.59.

The pulse was calibrated through the following steps: (1) Using Bloch equations, the spectral response of the

pulse was calculated as a function of the peak B_1 amplitude to find the threshold value of the peak amplitude to function; (2) the corresponding voltage was determined; and (3) an overdrive factor was defined as a scaling factor multiplied by the flip angle to drive the pulse with higher voltages. Therefore, an overdrive factor (OF) of 1 is the minimum peak voltage required for the pulse to function and was found to be 10 μ T for our experimental conditions. The OF provides a degree of freedom to control the power of the pulse, which is important for MTC, as the saturation

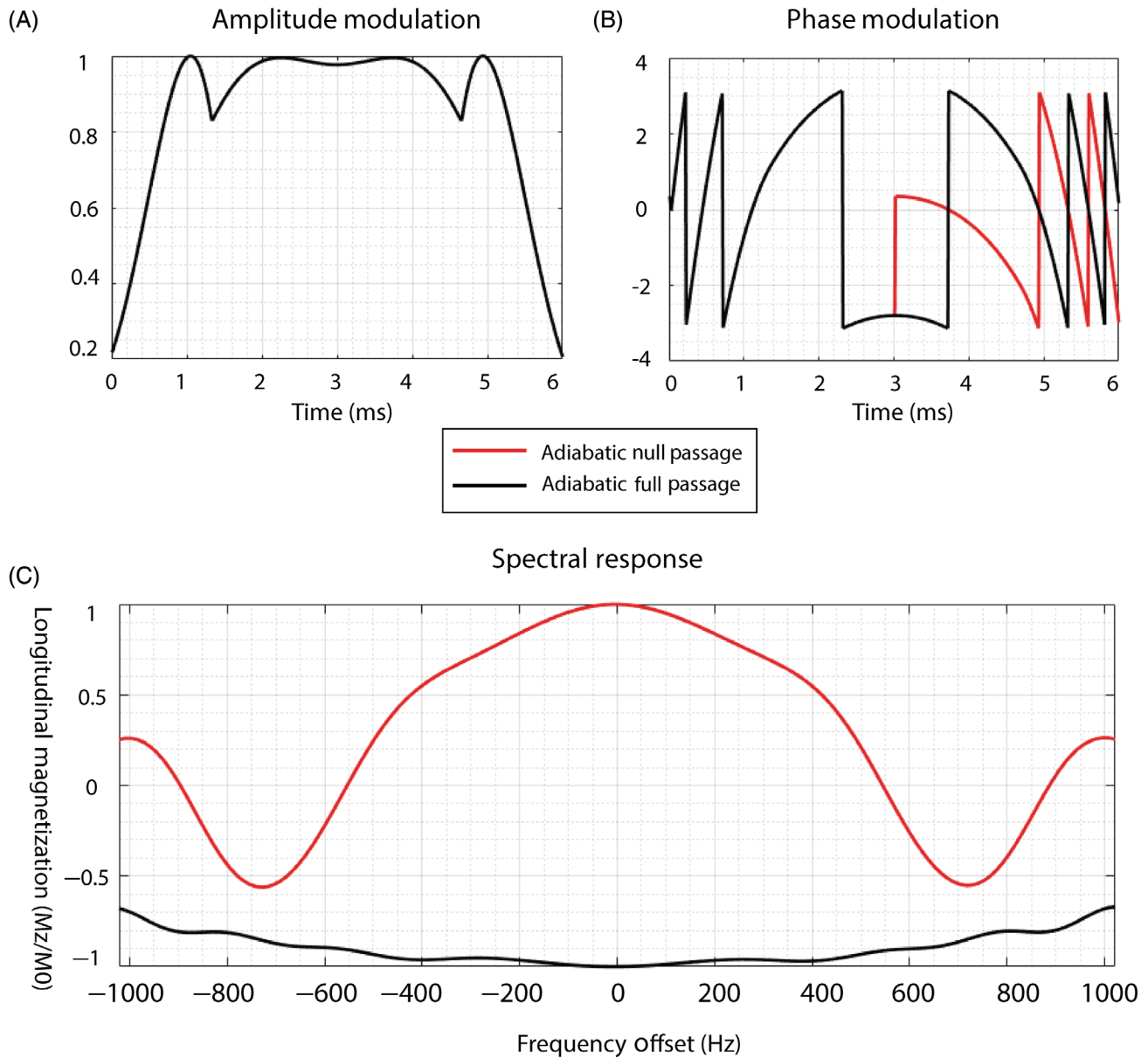


FIGURE 2 (A) The amplitude-modulation function for a 6-ms time-resampled frequency offset-corrected RF pulse is similar for both adiabatic full passage (AFP) and adiabatic null passage (ANP) cases. (B) The phase-modulation functions result in adiabatic null (red) and full (black) passages. (C) The spectral response over a 2000-Hz range of the frequency offsets for ANP (red) and AFP (black) scenarios.

of the bound pool and hence the MT-induced reduction in the magnetization of the free pool depends on the power of the MT pulse.

3.2 | Simulation

Binomial modulation for the RF pulse is the optimum candidate for on-resonance MT preparation. Davies et al.⁴³ identified a dark band artifact in the MTC images produced by a $1\bar{2}1$ binomial pulse and proposed that the repetition of the pulse train with a phase-inverted replica removes the artifact. Therefore, we compared our

proposed ANP pulse with a 6-ms phase-inverted $1\bar{2}1$ - $1\bar{2}1$ binomial pulse. In the simulation, we compared the sensitivity of the saturation bandwidth of these two pulses to the B_0 and B_1^+ inhomogeneity. We also compared their MT efficiency by evaluating the direct saturation and T_2 effect in the context of a practical pulse sequence.

3.2.1 | B_0 inhomogeneity

The performance of the binomial pulses is vulnerable to B_0 inhomogeneity. After obtaining written informed consent, we measured B_0 field maps for 7 healthy participants

using a vendor-provided dual-echo gradient-echo pulse sequence with TEs of 2.2 and 4.6 ms. The results indicated that the subject-dependent tissue-induced B_0 inhomogeneity causes the frequency of the free pool to be in a range of -350 to 350 Hz. Rather than measuring the FWHM of the distribution, a common practice reported in the literature, we considered the extreme values of the field maps to account for all possible variations. It is ideal if the null bandwidth of the pulse is larger than the water-fat shift (≈ 440 Hz at 3 T) so that the fat signal would not be reduced and hence misinterpreted as an MT-induced reduction. Therefore, the MT pulse requires a null bandwidth (transparent region) of about 880 Hz around the Larmor frequency. Because the null bandwidth is dependent on the power of the pulse, the independent variable affecting the null bandwidth is the flip angle for binomial pulses and the OF (a multiplicative factor determining how much power we are using above the adiabaticity of the pulse) for adiabatic pulses. To assess the saturation performance of the MT pulse, we simulated the spectral response of the pulses for different flip angles (FAs) of the shortest subpulse (45, 75, 90, and 107) of the binomial and overdrive factors (1, $\sqrt{2}$, $\sqrt{3}$, and $\sqrt{4}$) of the ANP pulse, with the same durations.

3.2.2 | B_1^+ inhomogeneity

In general, for any composite pulse with a phase difference of π , the magnetization response is independent of the flip angle for on-resonance spins. However, off-resonance, the jump-and-return principle of the binomial pulse, is compromised, and this makes it vulnerable to B_1^+ inhomogeneity.³¹ To evaluate the sensitivity of our technique to B_1^+ inhomogeneity, we simulated the magnetization response of two isochromat of spins precessing at 100 and 240 Hz off-resonance (arbitrarily chosen as representatives of low and high off-resonance populations) as a function of FA and overdrive factor for binomial and ANP, respectively.

3.2.3 | MT, direct saturation, and T_2 effect

For simulating the MT-related response of the pulses, we first need a model for the tissue to determine the exchange behavior among different pools of protons. We assumed the two-pool model for the brain tissue, which is used widely in literature. We then used Bloch-McConnell equations to simulate our in vivo experiment and calculate the contamination of the achieved MT effect with direct saturation and T_2 relaxation produced by trains of MT preparation pulses (binomial and ANP). The two-pool

TABLE 1 The two-pool model parameters for gray matter and white matter at 3T field strength. The values are used in Bloch-McConnell simulations.

Model parameter	Gray matter	White matter
M_{0b} (arbitrary unit)	0.072	0.161
k_{ab} (s^{-1})	2.4	4.3
T_{1a} (ms)	1075	555
T_{2a} (ms)	56	37
T_{2b} (μs)	11	12.3

model and the Bloch-McConnell equations are explained briefly as follows.

Two-pool model

We assume that protons of the tissue exist in two pools. One is an on-resonance narrowband pool of freely moving protons (free water molecules and protons in lipid structure) in the liquid state, and the other one is an on-resonance broadband pool of restricted protons (bound water, protons in the structure of macromolecules like proteins, and cell membranes) in the semisolid state. We use the terms “liquid” or “free” and “semisolid” or “bound” for referring to them throughout this article with “a” and “b” subscripts in the mathematical descriptions. The equilibrium magnetizations of the pools are M_{0a} for the liquid pool, M_{0b} for the semisolid pool, and $F = M_{0b}/M_{0a}$ is the pool size ratio. There is an exchange of magnetization between the two pools referred to as k_{ab} (rate constant pool a to b) and k_{ba} in the reverse direction. We can write $k_{ba} = k_{ab}/F$, because the exchange rate depends on the difference of the magnetizations. Each pool is characterized by its intrinsic relaxation parameters, which are T_{1a} , T_{2a} , T_{1b} , and T_{2b} . The MT models are not sensitive to the T_1 value of the semisolid pool; therefore, it is assumed to be 1 s (based on the estimated correlation time of the dipolar spin).²⁹ For gray matter and white matter at 3 T, the model is well-characterized, and the values are summarized in Table 1 taken from Sled and Pike.¹¹

Bloch-McConnell simulation

Bloch-McConnell equations extend the Bloch equations according to the two-pool model and quantitatively describe the behavior of the magnetization through the coupled set of equations stated in the matrix form as

$$\frac{d\vec{M}}{dt} = A \cdot \vec{M} + \vec{C} \quad (4)$$

where $\vec{M} = [M_{xa}, M_{ya}, M_{za}, M_{xb}, M_{yb}, M_{zb}]$ is the combined magnetization vector for liquid (a) and semisolid pool (b); $\vec{C} = [0, 0, R_{1a}M_{0z}, R_{1b}M_{0b}]$ is given by longitudinal rates and

equilibrium magnetizations; and A is a 4×4 matrix^{44–48} as follows:

$$A = \begin{vmatrix} -R_{2a} & -\Delta\omega_a & -\omega_{1y} & 0 \\ +\Delta\omega_a & -R_{2a} & +\omega_{1x} & 0 \\ +\omega_{1y} & -\omega_{1x} & -R_{1a} - k_{ab} & k_{ba} \\ 0 & 0 & k_{ab} & -R_{1b} - R_{rfb} - k_{ba} \end{vmatrix} \quad (5)$$

Where ω_1 represents the amplitude of the RF pulse; $\Delta\omega$ is the RF pulse offset relative to the Larmor frequency; $k_{ab/ba}$ the magnetization exchange rate; R_1 and R_2 are the relaxation rates; and R_{rfb} is the rate of saturation of the semisolid pool caused by the applied MT pulse, as follows:

$$R_{rfb} = \pi \frac{1}{T} \int_0^T \omega_1^2(t) dt \cdot G \quad (6)$$

where T is the pulse duration; $\omega_1(t)$ is the waveform of the MT pulse; and G is absorption line-shape of the semisolid pool. The transverse component of the semisolid pool magnetization is negligible due to the very short T_2 of the protons, as they are restricted to the structure of the macromolecules.⁴⁹ We used the super-Lorentzian absorption line shape, which is shown to provide the best approximation for biological tissues.⁵⁰

As Eq. (6) suggests, MT pulses with the same power saturate the semisolid pool at the same rate; therefore, they provide an identical amount of MT-related contrast in the tissue. To compare the performance of the binomial pulse with the ANP MT preparation, we simulated the pulse sequence using two power-matched MT pulses generating the same amount of MT. Therefore, it allowed us to estimate the contamination of their MT performance with direct saturation and T_2 relaxation effect.

3.3 | Experiment

Imaging was performed on a 3T scanner (Prisma; Siemens Healthineers, Erlangen, Germany) with the 32-channel head coil. We compared the MT performance of our proposed ANP pulse (6 ms) with a phase-inverted $1\bar{2}1\text{--}1\bar{2}1$ binomial scheme³ (6 ms) with the MT preparation module in both cases followed by a simple 2D multislice EPI readout. Figure 3 shows the diagram for the pulse sequences, with different MT preparation pulses. The imaging parameters were FOV = 240×240 mm², TR = 1800 ms, TE = 11 ms, GRAPPA = 2, slice thickness = 3 mm, and partial Fourier = 6/8. Base matrix size was set to 80, achieving 3-mm isotropic resolution. A total of 30 slices were acquired in each volume with the interslice TR of 59 ms. The pulse repetition period (PRP) was defined as the time

between two successive MT pulses, and the value is a multiple of the slice TR, depending on the protocol. For each experiment, we acquired 40 volumes: the first 20 volumes without the MT pulse (providing a reference image) and the second 20 volumes with the MT pulse. To ensure that the MT-related equilibrium is achieved, and the MTC is built up, we chose the 40th volume as the MT-weighted image. The 20th volume was used as the reference image. A field map was also acquired using a simple dual-echo gradient-echo sequence with TEs of 2.2 and 4.6 ms with the same FOV, resolution, and slice position as the MTC volumes. We obtained written informed consent from the 3 participants as approved by the local human ethics committee (Committee on Research Involving Human Subjects, Region Arnhem-Nijmegen, the Netherlands).

3.4 | Image analysis

To show the MT-induced reductions due to the saturation of the semisolid, we calculated magnetization transfer ratio (MTR) maps for each experiment (participant). The MTR values were calculated as $1 - (\text{MT-weighted intensity/reference intensity})$ for each voxel inside the brain to obtain the MT map. Before the MTR calculation, several processing steps were performed: (1) The whole 40-volume scan was realigned based on the midvolume using *mcflirt* in FSL for motion correction; (2) the images were corrected for bias field due to the receive coil sensitivity profile using *SPM*; and (3) the brain was masked using *BET*, and gray matter (GM), white matter (WM), and CSF were segmented using *SPM*. Given that CSF is a non-MT-active tissue with a long T_1/T_2 , we looked at the CSF signal as a reliable site to observe direct saturation. Therefore, for this analysis, we plotted an average of line profiles passing through CSF in the lateral ventricles of the brain, which provides a comparison of the MTR values in GM, WM, and CSF.

4 | RESULTS

Figure 4A–D shows the comparison of the spectral responses for a 6-ms ANP and a 6-ms phase-inverted binomial pulse train for different FAs and OFs. The green band of frequency is the ideal null bandwidth that we expect to achieve at 3 T. Although no pulse can achieve the ideal, the figure shows clearly that the fluctuations inside the green band are reduced considerably with the ANP pulse, indicating improved sensitivity of the saturation performance toward B_0 inhomogeneity for the ANP pulse.

Figure 4E,F shows the longitudinal magnetization as a function of FA and OF for binomial and ANP

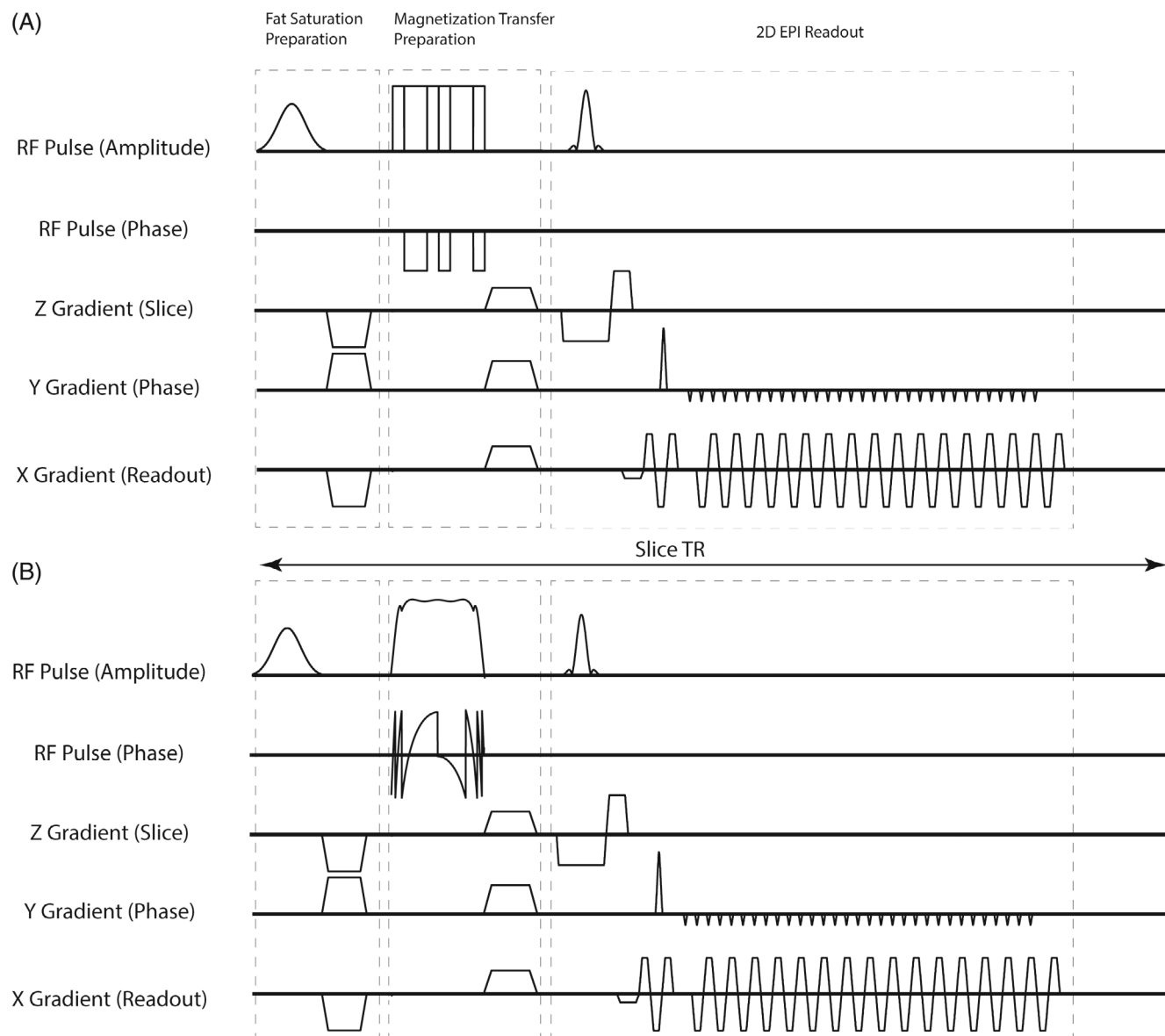


FIGURE 3 The pulse sequence used to generate the magnetization-transfer contrast with a $121-121$ binomial scheme (A) and with our proposed adiabatic null passage pulse (B). This scheme repeats by the number of slices (30) in a volume TR of 1800 ms.

pulses, respectively, for two isochromat of spins with offset frequencies of 100 and 240 Hz. At offset frequencies as low as 100 Hz, both ANP and binomial pulses are almost immune to B_1^+ variations, with about 10% variations in the magnitude. At higher frequency offset values, the pulse performance deteriorates, showing larger oscillations. However, the results clearly show that despite the oscillations (about 20% in magnitude), the overall trend of the magnetization shows a higher level of robustness to B_1^+ variations for the ANP pulse at large frequency-offset values compared with the binomial pulse. This suggests that our proposed technique performs the jump-and-return of the spins slowly and adiabatically, which makes it robust to alterations in the RF amplitude.

Figure 5A shows the evolution of the longitudinal magnetization of the liquid pool for a certain slice during the repetitive application of the MT pulse, which is calculated using the established two-pool model for GM (Table 1) and through Bloch-McConnell simulations (Eq. [6]). The simulation is done for four power-matched protocols and each for two volumes (volume TR = 1.8 s) with 30 slices per volume (slice TR = 59 ms). The MT pulse is followed by a 4-ms spoiler gradient. Figure 5B shows a zoomed view of the simulation for the duration of six TR_{slice}. The temporal resolution of the simulation point varies during the simulated volume. From Points A to B, which takes 6 ms, seven time points are used to depict the evolution of the magnetization through the application of the MT

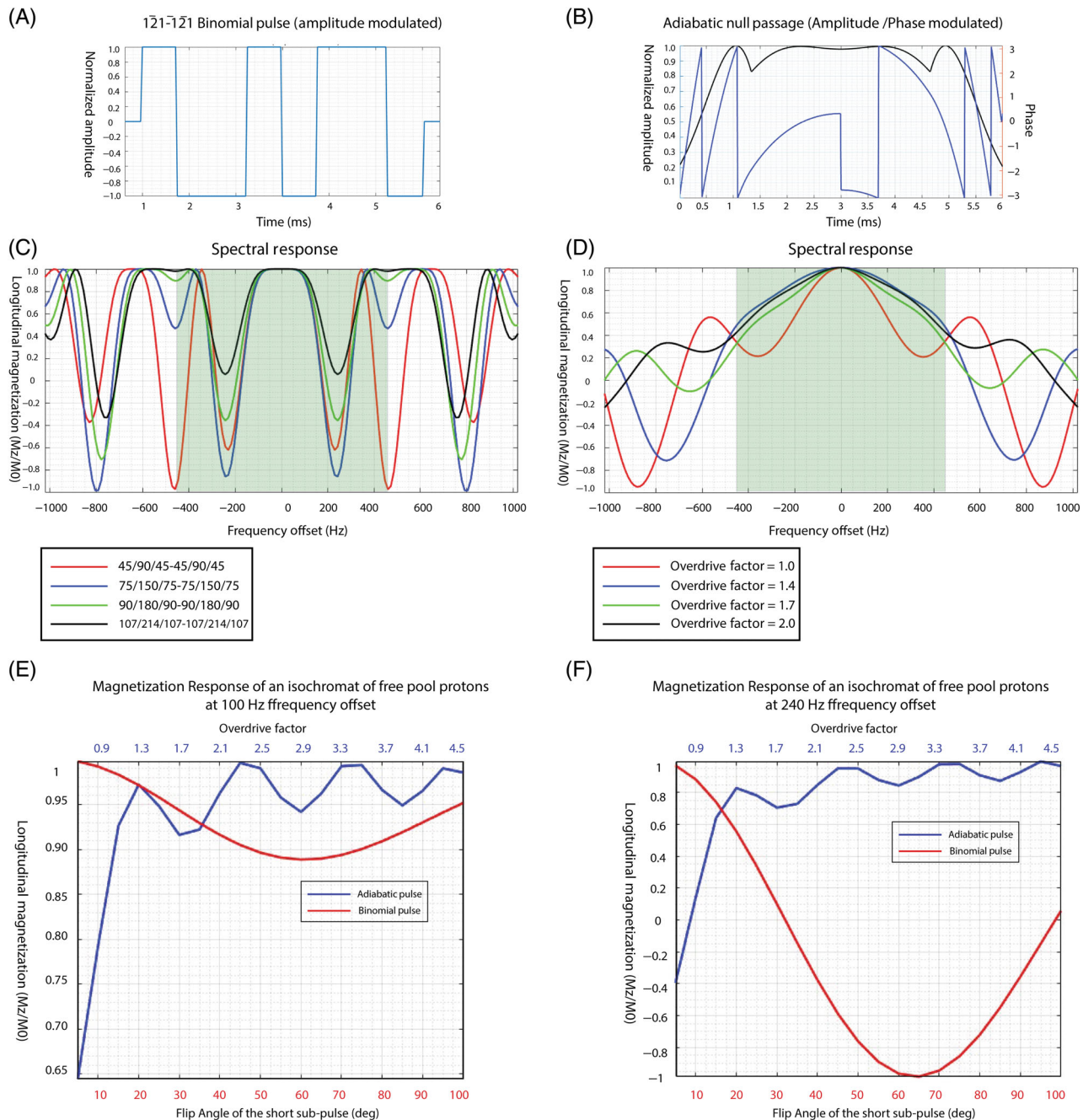


FIGURE 4 The saturation performance of $121\text{-}\bar{1}21$ binomial (A) and our proposed adiabatic null passage (ANP) pulse (B) are compared by showing their spectral response. The green area shows the range of frequency offsets of the free pool protons in a human head at 3 T. The spectral responses are shown for different flip angles (FAs) for the binomial pulse (C) and various overdrive factors for the ANP pulse (D). The longitudinal magnetization as a function of FA (of the shortest subpulse) and the overdrive factor for binomial (red) and ANP (blue) pulse for an isochromat of spins at 100 Hz (E) and 240 Hz (F) off-resonance.

pulse. High temporal resolution is used to visualize the jump-and-return of the spins, whereas from Points C to D, which is the duration of the readout for the whole slice (47 ms), only two time points are depicted. Lower temporal resolution was used, as nothing other than simple relaxation happens during this period. The time between Points B to C relates to the spoiler gradient and takes 3 ms.

The power of the MT pulse is balanced with the pulse repetition period (PRP values of TR, 2TR, and 3TR correspond to OFs of 1, $\sqrt{2}$, and $\sqrt{3}$, respectively) so that all four protocols have identical power. This guarantees a fixed rate for the saturation of the semi-solid pool and therefore the same amount of MT-induced reduction in the signal. At the beginning of each volume, there is a

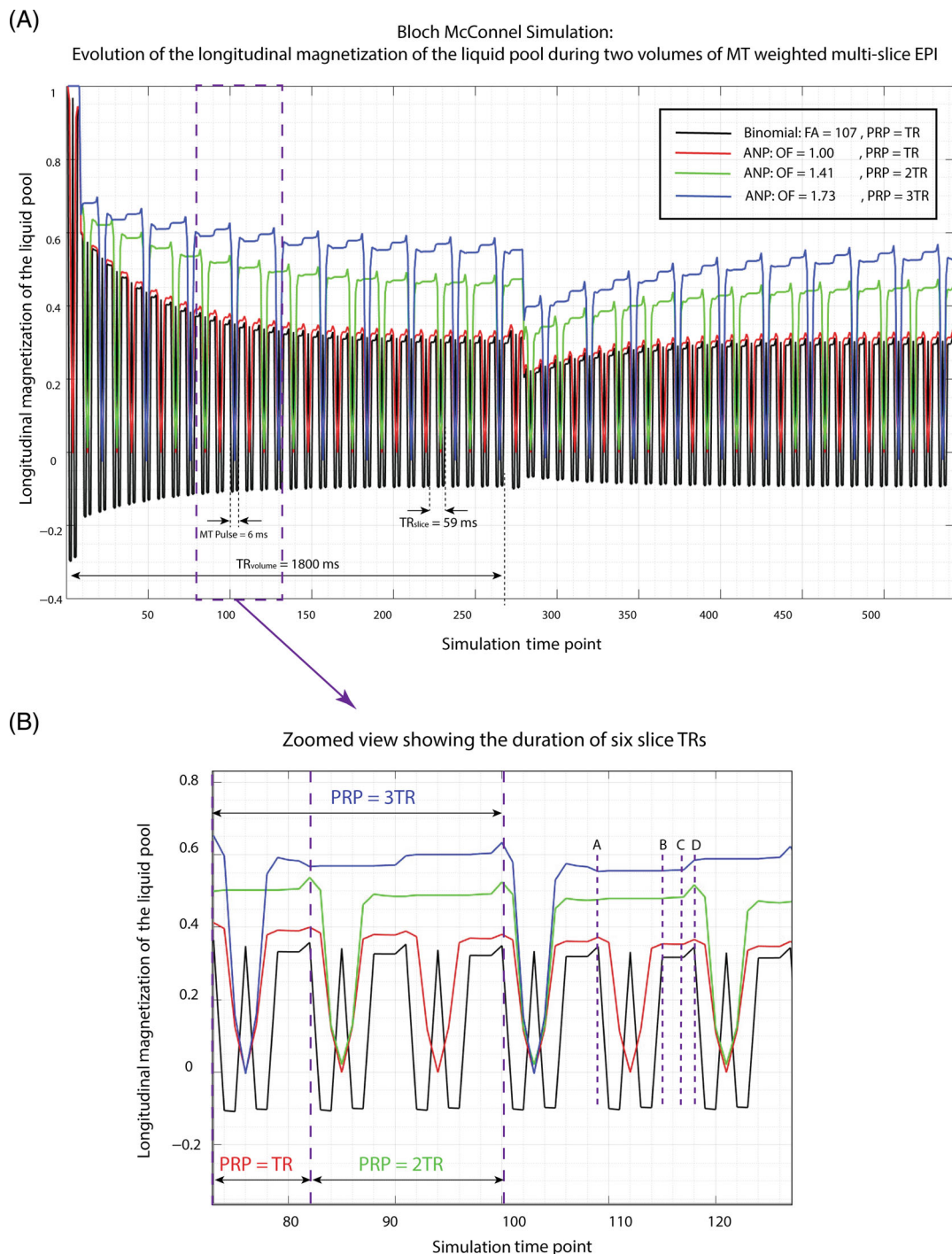


FIGURE 5 (A) Bloch-McConnell simulation of two volumes of the magnetization transfer (MT)-weighted multislice EPI sequence. Four different power-matched scenarios are shown: (1) a phase-inverted $\hat{1}\hat{2}\hat{1}$ - $\hat{1}\hat{2}\hat{1}$ binomial with a flip angle of 107 for the shortest subpulse applied at every slice (black), (2) a 6-ms adiabatic null passage (ANP) pulse with an overdrive factor of 1 applied at every slice (red), (3) a 6-ms ANP pulse with an overdrive factor of 1.41 applied once every two slices (green), and (4) a 6-ms ANP pulse with an overdrive factor of 1.73 applied once every three slices (blue). (B) A zoomed view of the simulation for the duration of six slice TRs. PRP, pulse repetition period.

rather large reduction in the magnetization, which is the result of an excitation pulse. Because the excitation is slice-selective, it is applied once per volume as opposed to the nonselective MT pulse, which is applied for all slices in the volume. The MT effect of the other excitation pulses

that are off-resonance to the target slice as well as the fat saturation pulse for simulation was neglected.

Without MT preparation, the longitudinal magnetization reaches the steady state approximately after four volumes due to the $T_{1,obs}$ relaxation time. However, in the

presence of the MT, the newly established equilibrium reaches a different relaxation time known as $T_{1,\text{sat}}$, which is shorter than $T_{1,\text{obs}}$. Simulations showed the establishment of a steady state after two volumes. As shown in Figure 5, the black (binomial) and red (ANP with OF = 1) diagrams behaved similarly; however, the available magnetization at steady state increases by increasing PRP (green and blue diagrams), indicating reduced T_2 contamination.

The MTR values (mean + SD across all slices across the 3 participants) were both simulated and measured in vivo and are reported for the four power-matched scenarios in Table 2. The simulated and measured values are in relatively good agreement with the expected small discrepancies. Table 2 indicates that ANP with PRP = 3 TR and an OF of 1.73 reduces the T_2 effect by 19% in GM tissue and by 16% in WM tissue. As Figure 4A–D suggests, this improvement is pronounced off-resonance due to the improved null bandwidth of the ANP pulse. The simulated values for an off-resonant isochromat of spins precessing at the frequency of 240 Hz indicated that the T_2 /direct effect contamination is reduced by 22% in GM and by 24% in WM.

Figure 6 shows the MTR map of three exemplary slices acquired using a 6-ms ANP pulse applied with the PRP = 2TR and OF = $\sqrt{2}$, as well as the MTR maps of segmented GM, WM, and CSF. As expected, the MTR is high at WM due to the presence of a higher concentration of macromolecules, is slightly lower at GM, and is low at CSF.

Figure 7 shows the MTR maps for a 6-ms ANP pulse in three different settings along with the average line MTR profiles. The ANP OF and PRP parameters are chosen in the way that all three experiments are power-matched, so that the amount of liquid pool direct saturation and T_2 effect can be observed without any bias. The MTR values across the red line depict a high MTR at GM/WM with close to zero values for voxels containing CSF.

Figure 8 compares the MT performance of the binomial pulse with our proposed optimal adiabatic pulse in an in vivo experiment at regions with high B_0 inhomogeneity. Excessive direct saturation/ T_2 effect is observed in the

areas with high B_0 inhomogeneity (red arrow) in the binomial MTC images, whereas in the ANP-MTC images it is improved.

5 | DISCUSSION

We proposed a new adiabatic pulse, termed an adiabatic null passage (ANP), that generates zero FA by reversing the phase modulation function at its midpoint, making the bulk magnetization return to its parallel state with the static field. We demonstrated its performance as an on-resonance magnetization preparation module in an EPI sequence. We showed that the ANP pulse provides a wider null bandwidth in the spectral response, improving its performance at the existence of B_0 inhomogeneity. Therefore, the direct saturation of the liquid pool, which is exacerbated at off-resonance due to failure of the jump-and-return of the magnetization, is improved. We showed that above a threshold (adiabatic condition), the trajectory of the spins (as well as the FA) during the ANP is independent of the power. This could be exploited to apply the MT pulse less often (PRP = 2 TR or 3 TR) compared with binomial pulses, which reduces the T_2 contamination of the MT.

Although the routine clinical neuroimaging application of MTC is limited to angiography,⁵¹ it is helpful in a wide spectrum of special applications such as multiple sclerosis classification,⁵² osteoarthritis and cartilage evaluation,⁵³ coronary arteries examination,⁵⁴ and Crohn's disease characterization.⁵⁵ The contrast is predicated following the significant signal reduction of the MT-active voxels (e.g., WM, GM, skeletal muscle, myocardium, cartilage, liver) versus ideally no signal reduction in the MT-inactive voxels (e.g., CSF, adipose tissue, bone marrow, blood). However, two unwanted mechanisms could induce a reduction in the magnetization value of MT-inactive voxels degrading the desired contrast. The first is direct saturation of the liquid pool and the second is the T_2 relaxation during the repetitive application of the MT

TABLE 2 The measured and simulated magnetization transfer ratio values were achieved with the pulse sequence shown in Figure 3 and in gray-matter and white-matter tissues using four power-matched magnetization-transfer preparation schemes.

Magnetization transfer pulse	Gray matter		White matter	
	In vivo	Simulation	In vivo	Simulation
Binomial (FA = 107, PRP = TR)	58% ± 2%	66%	63% ± 1.5%	62%
ANP (OF = 1, PRP = TR)	61% ± 3.8%	64%	64% ± 2.7%	61%
ANP (OF = $\sqrt{2}$, PRP = 2TR)	46% ± 1.8%	53%	51% ± 0.7%	52%
ANP (OF = $\sqrt{3}$, PRP = 3 TR)	38% ± 1.1%	45%	42% ± 1.4%	45%

Abbreviations: ANP, adiabatic null passage; FA, flip angle; OF, overdrive factor; PRP, pulse repetition period.

Magnetization Transfer Ratio Maps generated by 6-ms ANP pulse with PRP = 2TR, OF = 1.41

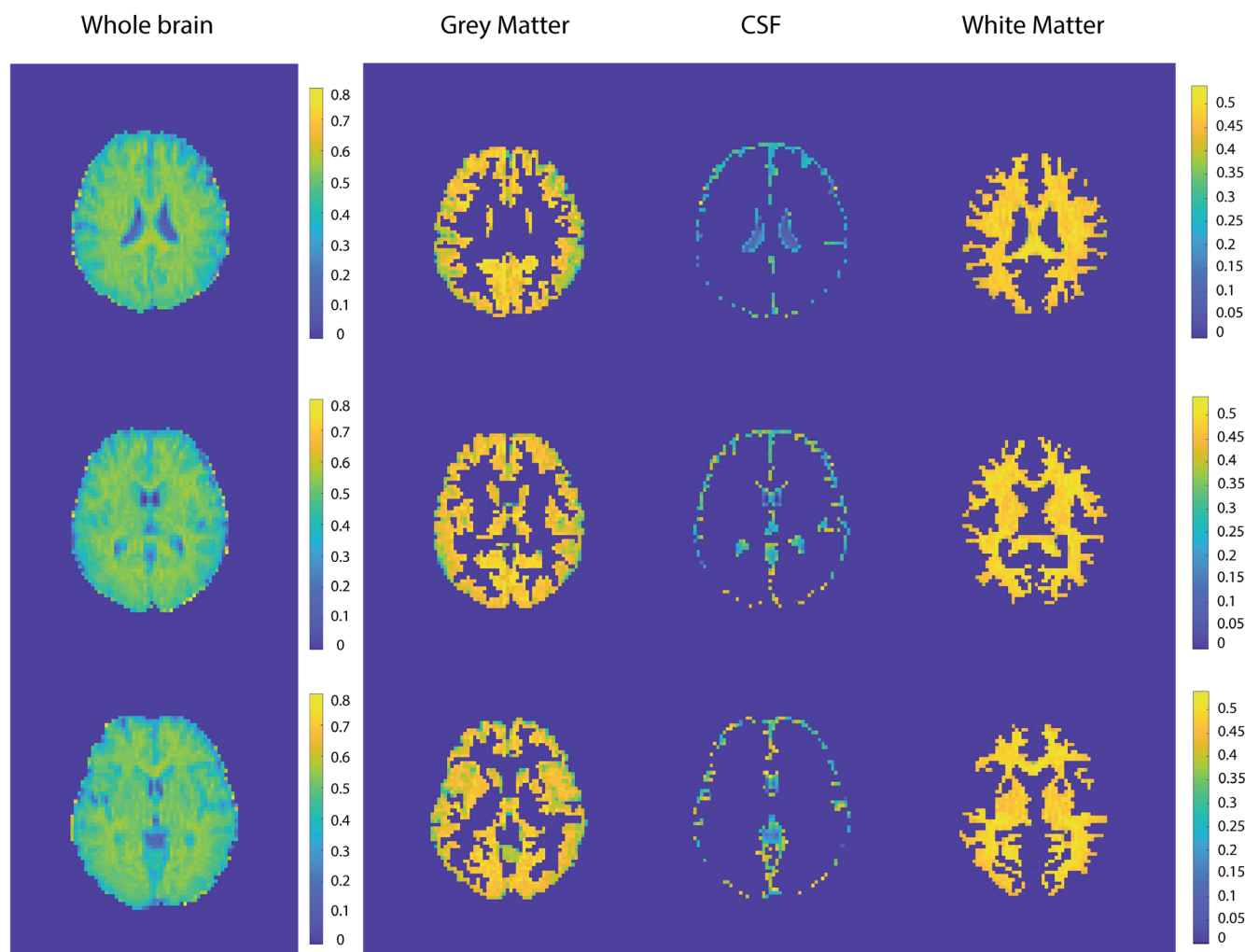


FIGURE 6 Three exemplary slices of the magnetization transfer ratio maps were acquired using a 6-ms adiabatic null passage (ANP) pulse at the pulse repetition period (PRP) of 2TR and overdrive factor (OF) of 1.41. The MTR maps are shown for gray matter, white matter, and CSF separately.

preparation pulse interleaved with the imaging pulse sequence. Although disentanglement of these two effects is rather complicated, we showed in both simulation and in vivo that our technique reduced these unwanted effects, which improves the MTC offered by this technique.

Almost any train of short hard pulses and delays produces a complicated trajectory for the long- T_2 magnetization (liquid), which could land back parallel with the static field, during which the short- T_2 components (semisolid pool) would have decayed. This is the so-called jump-and-return idea behind binomial amplitude modulation for an on-resonance MT pulse.²⁵ However, many experimental imperfections could prevent this from working as intended.⁴³ Furthermore, tedious optimization of a range of experimental parameters such as the number of subpulses, pulse length, phase shift, peak amplitude, and delays are generally needed for a satisfactory result.^{31–33}

We showed that the saturation performance of the ANP pulse is superior in the presence of B_0 (Figures 8 and 4C) and B_1^+ (Figure 4E) inhomogeneity compared with the phase-inverted binomial counterpart. In our power-matched investigation (in vivo, Figure 7; simulation, Figure 5), we showed that the MTR value decreases using higher PRP, which provides a more reliable MTR value. The true MTR depends on the power per unit time and the offset frequency of the MT pulse. Because the experiments were power-matched and the pulses were applied on resonance, one could clearly associate the decrease in measured MTR with mitigating one of the two unwanted mechanisms: direct saturation and the T_2 effect. On resonance, as shown in the simulated spectral response of the pulses (Figures 2 and 4), the direct saturation could be considered almost zero. Therefore, one could hold T_2 accountable for all the contamination of the MT.

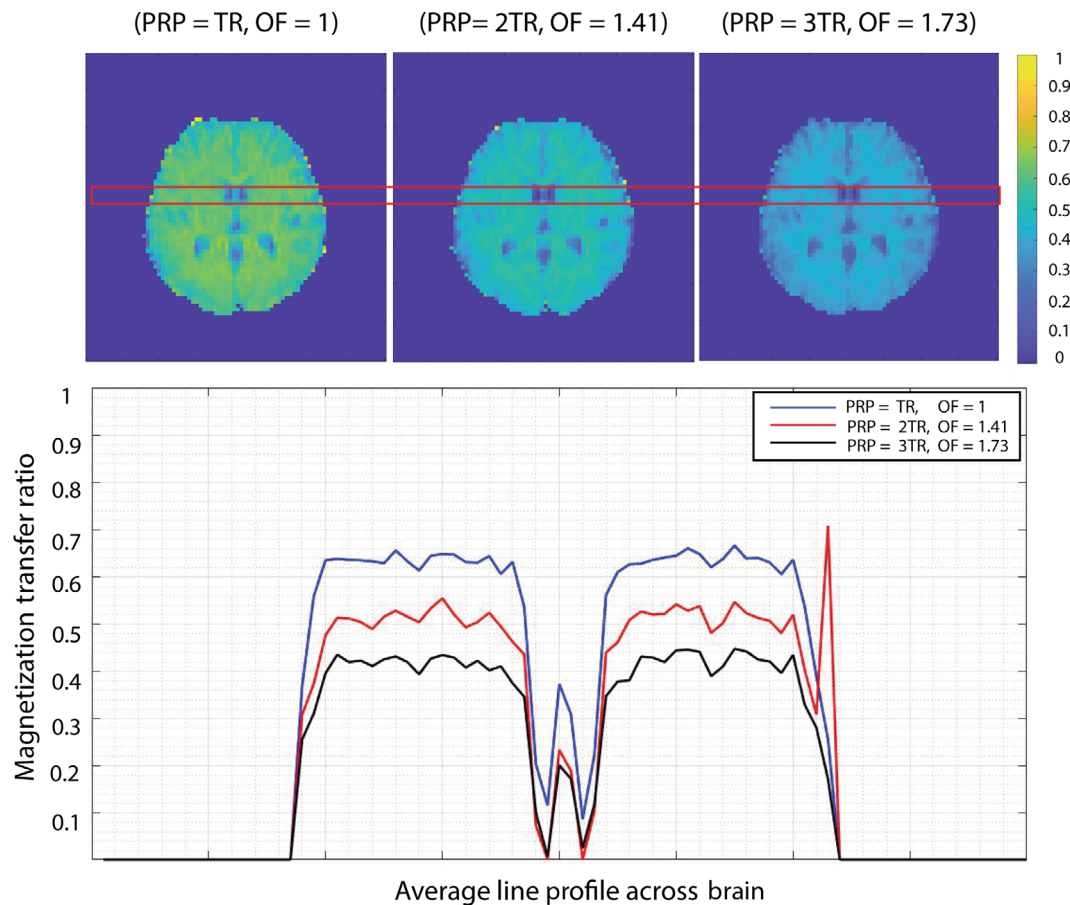


FIGURE 7 The magnetization transfer ratio maps were acquired using an adiabatic null passage (ANP) pulse in three different power-matched settings. OF, overdrive factor; PRP, pulse repetition period.

Off-resonance, however, the separation of T_2 and direct effect is not easy, and the two effects both contaminate the MT.

The T_2 effect depends on the amount of time that spins spend in the transverse plane, which reduces the signal through relaxation, and is maximized for the binomial-modulated pulse train with $FA = 90^\circ$. However, using binomial modulation with any FA still forces the spins to spend a considerable amount of time in the transverse plane. Although this also happens for the ANP and varies slightly with the OF, we showed in simulations (Figure 5) that a higher PRP value used with the ANP setting makes spins spend less time in the transverse plane, which considerably reduces the T_2 contamination of MTR values.

At GM (WM) in vivo, the MTR reduced from 61% (64%) by applying ANP with $OF = 1$ and $PRP = TR$, to 38% (42%) by applying ANP with an $OF = \sqrt{3}$ and $PRP = 3 TR$, demonstrating the mitigation of T_2 /direct effect by 23% (22%). The Bloch-McConnell simulations showed these reductions to be 19% at GM (from 64% to 45%) and 17% at WM (from 61% to 45%). The discrepancy between simulation and in vivo experiments could be the result of the

parameters for the two-pool model not being determined individually and based on the literature values, which cannot incorporate intersubject variations.

One advantage of the ANP pulse over the binomial pulses is the ability to increase the power of the pulse without changing its duration. Applying the binomial pulses at longer PRPs requires increasing their power by lengthening their duration. Longer binomial pulses would pronounce the T_2 contamination and counteract the benefit achieved through the increase in the PRP. However, for the ANP pulses, increasing the power of the pulse is realized through the OF, and therefore is independent of the duration of the pulse and barely modifies the trajectory of the magnetization.

Another advantage of the ANP pulse is its improved performance for the off-resonance spin isochromat. On resonance, the pulse can easily achieve the null passage through the reversal of the phase. Off-resonance, however, the perfect null passage is not achievable, as the established effective B_1 field contains a $\frac{\Delta\omega}{\gamma} \vec{k}$ term that is not reversible with the phase of the pulse. However, as Figure 4 demonstrates, the failure of the null passage as we go off-resonance is slow and slight compared with the abrupt

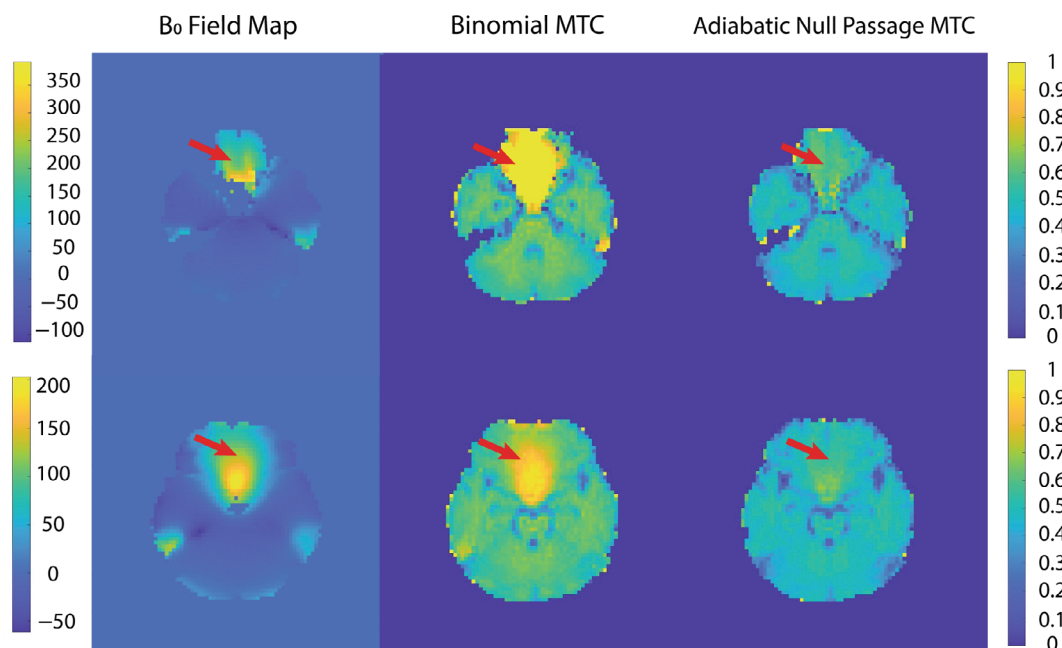


FIGURE 8 The magnetization transfer contrast (MTC) maps were acquired with two different pulses for magnetization transfer preparation. The left column shows the B_0 field maps. The MTC maps acquired with binomial pulse and adiabatic pulse are shown in the middle and right columns, respectively. The red arrows indicate the areas with high B_0 inhomogeneity, where the improvement is significant with adiabatic null passage.

failure of the null passage of the binomial pulses. Moreover, applying the ANP pulse at higher PRPs allows us to drive them with a higher power, which makes the dropout of the performance at off-resonance even slower.

A future direction for this study is to investigate the effect of pulse durations on the MT performance. Theoretically, MT pulses benefit from shorter durations, as they decrease the T_2 contamination. In practice, however, it entails technical challenges. Shorter durations for the adiabatic pulses make the adiabatic condition satisfied at a higher peak amplitude and exacerbates the SAR demand of the pulse. In addition to the SAR challenges, hardware restrictions of the RF amplifier might limit the use of shorter durations, as the required high peak voltage might be clipped, resulting in an inaccurate FA or OF. Further investigations are needed to seek an optimum trade-off between the pulse duration and the peak amplitude, which will probably be vendor-specific and system-specific.

The values for the OF of the ANP pulse and the FA of the binomial pulse determine the required peak voltage and hence the amount of energy deposition. Therefore, they are practically limited by SAR. Pulse voltages are calculated based on the reference transmitter voltage, which is automatically calibrated by the scanner based on the subject head size. Depending on the participant and the required transmitter voltage, an OF of up to 1.7 and shortest subpulse FA of up to 110° were possible in

our experiments. Achieving higher values might not be possible without prolonging the volume TR as compensation. Several SAR reduction strategies are proposed in the literature; however, the compromise of the SAR and the MT efficiency needs to be investigated before using the techniques.

Acquisition of 40 volumes to reach the steady-state equilibrium for the two-pool system is quite conservative, and for the sole purpose of MTC imaging, three volumes could be sufficient. However, we showed that a functional MRI protocol is also feasible with our proposed ANP pulse without any SAR-related restriction.

The improvement of the MT performance in the presence of both B_0 and B_1^+ inhomogeneity suggests promising application for ANP in MT-based techniques such as time-of-flight magnetic resonance angiography⁵⁶ and arterial blood contrast⁵⁷ functional MRI studies.

ORCID

Shahrokh Abbasi-Rad  <https://orcid.org/0000-0003-0964-485X>

David G. Norris  <https://orcid.org/0000-0002-3699-6917>

REFERENCES

- Edzes HT, Samulski ET. The measurement of cross-relaxation effects in the proton NMR spin-lattice relaxation of water in biological systems: hydrated collagen and muscle. *J Magn Reson*. 1978;31:207-229.

2. Koenig SH, Bryant RG, Hallenga K, Jacob GS. Magnetic cross-relaxation among protons in protein solutions. *Biochemistry*. 1978;17:4348-4358.
3. Alger J, Prestegard P. Investigation of peptide bond isomerization by magnetization transfer NMR. *J Magn Reson*. 1977;27:137-141.
4. Forsén S, Hoffman RA. Study of moderately rapid chemical exchange reactions by means of nuclear magnetic double resonance. *J Chem Phys*. 1963;39:2892-2901.
5. Grad J, Bryant RG. Nuclear magnetic cross-relaxation spectroscopy. *J Magn Reson*. 1990;90:1-8.
6. Zhong J, Gore JC, Armitage IM. Quantitative studies of hydrodynamic effects and cross-relaxation in protein solutions and tissues with proton and deuteron longitudinal relaxation times. *Magn Reson Med*. 1990;13:192-203.
7. Eng J, Ceckler TL, Balaban RS. Quantitative ¹H magnetization transfer imaging in vivo. *Magn Reson Med*. 1991;17:304-314.
8. Fung B. [10] Nuclear magnetic resonance study of water interactions with proteins, biomolecules, membranes, and tissues. *Methods Enzymol*. 1986;127:151-161.
9. Campbell ID, Dobson CM, Ratcliffe RG, et al. Fourier transform NMR pulse methods for the measurement of slow-exchange rates. *J Magn Reson*. 1978;29:397-417.
10. Wolff SD, Balaban RS. Magnetization transfer contrast (MTC) and tissue water proton relaxation in vivo. *Magn Reson Med*. 1989;10:135-144.
11. Sled JG, Pike GB. Quantitative imaging of magnetization transfer exchange and relaxation properties in vivo using MRI. *Magn Reson Med*. 2001;46:923-931.
12. Chai JW, Chen C, Chen JH, Lee SK, Yeung HN. Estimation of in vivo proton intrinsic and cross-relaxation rates in human brain. *Magn Reson Med*. 1996;36:147-152.
13. Rope S, Stollberger R, Hartung HP, Fazekas F. Estimation of magnetization transfer rates from PACE experiments with pulsed RF saturation. *J Magn Reson Imaging*. 2000;12:749-756.
14. Edelman R, Ahn SS, Chien D, et al. Improved time-of-flight MR angiography of the brain with magnetization transfer contrast. *Radiology*. 1992;184:395-399.
15. Wolff SD, Chesnick S, Frank JA, Lim KO, Balaban RS. Magnetization transfer contrast: MR imaging of the knee. *Radiology*. 1991;179:623-628.
16. Finelli DA, Hurst GC, Karaman BA, Simon JE, Duerk JL, Bellon EM. Use of magnetization transfer for improved contrast on gradient-echo MR images of the cervical spine. *Radiology*. 1994;193:165-171.
17. Kelly DAC, Graham R, Kappler F, Kowalyshyn M, Keller S, Brown TR. Magnetisation transfer contrast imaging at 2.3 T. In: *Proceedings of the 8th Annual Meeting of ISMRM*. Society of Magnetic Resonance in Medicine (SMRM); 1989: 1036.
18. Wolff SD, Eng J, Balaban R. Magnetization transfer contrast: method for improving contrast in gradient-recalled-echo images. *Radiology*. 1991;179:133-137.
19. Dixon WT, Engels H, Castillo M, Sardashti M. Incidental magnetization transfer contrast in standard multislice imaging. *Magn Reson Imaging*. 1990;8:417-422.
20. Ordidge RJ, Knight RA, Helpen J. Magnetization transfer contrast (MTC) in flash MR imaging. *Magn Reson Imaging*. 1991;9:889-893.
21. Ordidge RJ, Helpen JA, Knight RA, Qing Z, Welch KMA. Investigation of cerebral ischemia using magnetization transfer contrast (MTC) MR imaging. *Magn Reson Imaging*. 1991;9:895-902.
22. Hajnal JV, Baudouin CJ, Oatridge A, Young IR, Bydder GM. Design and implementation of magnetization transfer pulse sequences for clinical use. *J Comput Assist Tomogr*. 1992;16:7-18.
23. Outwater E, Schnall MD, Braitman LE, Dinsmore BJ, Kressel HY. Magnetization transfer of hepatic lesions: evaluation of a novel contrast technique in the abdomen. *Radiology*. 1992;182:535-540.
24. Pierce WB, Harms SE, Flamig DP, Griffey RH, Evans WP, Hagans JE. Three-dimensional gadolinium-enhanced MR imaging of the breast: pulse sequence with fat suppression and magnetization transfer contrast. *Radiology*. 1991;181:757-763.
25. Hore P. Solvent suppression in Fourier transform nuclear magnetic resonance. *J Magn Reson*. 1983;55:283-300.
26. Hu BS, Conolly SM, Wright GA, Nishimura DG, Macovski A. Pulsed saturation transfer contrast. *Magn Reson Med*. 1992;26:231-240.
27. Yeung HN, Aisen AM. Magnetization transfer contrast with periodic pulsed saturation. *Radiology*. 1992;183:209-214.
28. Hua J, Hurst GC. Analysis of on-and off-resonance magnetization transfer techniques. *J Magn Reson Imaging*. 1995;5: 113-120.
29. Graham S, Henkelman RM. Understanding pulsed magnetization transfer. *J Magn Reson Imaging*. 1997;7:903-912.
30. Pike GB, Glover GH, Hu BS, Enzmann DR. Pulsed magnetization transfer spin-echo MR imaging. *J Magn Reson Imaging*. 1993;3:531-539.
31. Schneider E, Prost RW, Glover GH. Pulsed magnetization transfer versus continuous wave irradiation for tissue contrast enhancement. *J Magn Reson Imaging*. 1993;3:417-423.
32. Schick F, Forster J, Pfeffer M, Lutz O. Pulsed magnetization transfer for imaging and spectroscopic applications on whole-body imagers. *Magn Reson Mater Phys Biol Med*. 1994;2:127-137.
33. Pachot-Clouard M, Darrasse L. Optimization of T₂-selective binomial pulses for magnetization transfer. *Magn Reson Med*. 1995;34:462-469.
34. Liang Z-P, Lauterbur PC. *Principles of Magnetic Resonance Imaging: A Signal Processing Perspective*. SPIE Optical Engineering Press; 2000.
35. Idema T. *Mechanics and Relativity*. 2018.
36. Bernstein MA, King KF, Zhou XJ. *Handbook of MRI Pulse Sequences*. Elsevier; 2004.
37. Baum J, Tycko R, Pines A. Broadband population inversion by phase modulated pulses. *J Chem Phys*. 1983;79:4643-4644.
38. Norris DG. 0° slice-selective RF pulses: MT-equivalence for multi-slice perfusion imaging. *Proceedings of the 6th Annual Meeting of ISMRM*, Sydney, Australia 1998.
39. Hurley AC, al-Radaideh A, Bai L, et al. Tailored RF pulse for magnetization inversion at ultrahigh field. *Magn Reson Med*. 2010;63:51-58.
40. Ordidge RJ, Wylezinska M, Hugg JW, Butterworth E, Franconi F. Frequency offset corrected inversion (FOCI) pulses for use in localized spectroscopy. *Magn Reson Med*. 1996;36:562-566.
41. Conolly S, Nishimura D, Macovski A, Glover G. Variable-rate selective excitation. *J Magn Reson*. 1988;78:440-458.

42. Abbasi-Rad S, O'Brien K, Kelly S, Vegh V, et al. Improving FLAIR SAR efficiency at 7T by adaptive tailoring of adiabatic pulse power through deep learning B_1^+ estimation. *Magn Reson Med*. 2020;85:2462-2476.
43. Davies NP, Summers IR, Vennart W. Optimum setting of binomial pulses for magnetization transfer contrast. *J Magn Reson Imaging*. 2000;11:539-548.
44. Zaiss M, Angelovski G, Demetriou E, McMahon MT, Golay X, Scheffler K. QUESP and QUEST revisited—fast and accurate quantitative CEST experiments. *Magn Reson Med*. 2018;79:1708-1721.
45. Zaiss M, Zu Z, Xu J, et al. A combined analytical solution for chemical exchange saturation transfer and semi-solid magnetization transfer. *NMR Biomed*. 2015;28:217-230.
46. Woessner DE, Zhang S, Merritt ME, Sherry AD. Numerical solution of the Bloch equations provides insights into the optimum design of PARACEST agents for MRI. *Magn Reson Med*. 2005;53:790-799.
47. Roeloffs V, Meyer C, Bachert P, Zaiss M. Towards quantification of pulsed spinlock and CEST at clinical MR scanners: an analytical interleaved saturation–relaxation (ISAR) approach. *NMR Biomed*. 2015;28:40-53.
48. Meissner JE, Goerke S, Rerich E, et al. Quantitative pulsed CEST-MRI using Ω -plots. *NMR Biomed*. 2015;28:1196-1208.
49. Wu X, Listinsky JJ. Effects of transverse cross relaxation on magnetization transfer. *J Magn Reson B*. 1994;105:73-76.
50. Li JG, Graham SJ, Henkelman RM. A flexible magnetization transfer line shape derived from tissue experimental data. *Magn Reson Med*. 1997;37:866-871.
51. Pike GB, Hu BS, Glover GH, Enzmann DR. Magnetization transfer time-of-flight magnetic resonance angiography. *Magn Reson Med*. 1992;25:372-379.
52. Dousset V. Magnetization transfer imaging in vivo study of normal brain tissues and characterization of multiple sclerosis and experimental allergic encephalomyelitis lesions. *J Neuroradiol*. 1993;20:297.
53. Welsch GH, Trattnig S, Scheffler K, et al. Magnetization transfer contrast and T2 mapping in the evaluation of cartilage repair tissue with 3T MRI. *J Magn Reson Imaging*. 2008;28:979-986.
54. Li D, Paschal CB, Haacke EM, Adler LP. Coronary arteries: three-dimensional MR imaging with fat saturation and magnetization transfer contrast. *Radiology*. 1993;187:401-406.
55. Li X-H, Mao R, Huang S-Y, et al. Characterization of degree of intestinal fibrosis in patients with Crohn disease by using magnetization transfer MR imaging. *Radiology*. 2018;287:494-503.
56. Schulz J, Boyacıoğlu R, Norris DG. Multiband multislab 3D time-of-flight magnetic resonance angiography for reduced acquisition time and improved sensitivity. *Magn Reson Med*. 2016;75:1662-1668.
57. Schulz J, Fazal Z, Metere R, Marques JP, Norris DG. Arterial blood contrast (ABC) enabled by magnetization transfer (MT): a novel MRI technique for enhancing the measurement of brain activation changes. 2020. doi:10.1101/2020.05.20.106666

How to cite this article: Abbasi-Rad S, Norris DG. Adiabatic null passage for on-resonance magnetization transfer preparation. *Magn Reson Med*. 2024;91:133-148. doi: 10.1002/mrm.29835